J. Fluid Mech. (1989), *vol.* 209, *pp.* 249–263
Printed in Great Britain

Long-time evolution and regions of existence of parametrically excited nonlinear cross-waves in a tank

By LEV SHEMER AND ELIEZER KIT
Department of Fluid Mechanics and Heat Transfer, Tel-Aviv University, Ramat-Aviv 69978, Israel

(Received 19 April 1988 and in revised form 1 March 1989)

Results of an experimental and numerical study of parametrically excited nonlinear cross-waves in the vicinity of the cut-off frequency, are reported. Experiments are performed at three cross-wave modes and in the whole range of existence of cross-waves. Numerical studies are based on the solution of the nonlinear Schrödinger equation with a boundary condition at the wavemaker which corresponds to parametric excitation. The validity of the scaling procedure adopted in the model is verified experimentally. Dissipation is incorporated in the model equation and in the wavemaker boundary condition. The influence of the wave breaking on the range of existence of cross-waves is discussed and the relation between the maximum possible steepness of cross-waves and the limits of their existence is obtained.

1. Introduction

Cross-waves are standing waves that appear in a rectangular wave tank equipped with a wavemaker, at the subharmonic of the forcing frequency due to parametric resonance (Garrett 1970; Mahony 1972). The inviscid model equation valid to the third order in the small parameter of the problem, ϵ, as well as the appropriate boundary conditions at the wavemaker, were first derived by Jones (1984). Miles (1984, 1985) and Miles & Becker (1988) rederived the governing equation using an entirely different approach and showed that it can be presented in the form of a nonlinear Schrödinger (NLS) equation. Lichter & Chen (1987) solved the NLS equation numerically, introducing into the model equation an additional term to account for dissipation along the tank. The dissipation term was estimated in accordance with the experimental study of the neutral stability of cross-waves by Barnard & Pritchard (1972). For a particular value of forcing amplitude and frequency Lichter & Chen obtained agreement between the period of long-time modulation in their numerical solution of the NLS equation and the experimental result of Barnard & Pritchard.

In the experiments of Lichter & Shemer (1986) additional modulated wave patterns, like propagating envelope solitons, were first observed. In a recent investigation, Shemer & Lichter (1987) performed a detailed experimental analysis of the fifth-mode cross-wave behaviour at various forcing frequencies and amplitudes. The neutral stability curve was also obtained in their work. The presentation of the experimentally obtained neutral stability curves of Barnard & Pritchard and of Shemer & Lichter, as the normalized dimensionless forcing amplitude ϵ *vs.* the detuning parameter λ, revealed qualitative differences between various experimental

facilities and modes of cross-waves (Kit & Shemer 1989). Kit & Shemer attributed this effect mainly to the dissipation at the wavemaker in the experimental facility used by Shemer & Lichter. The dissipation at the wavemaker was therefore incorporated in the model by modifying the boundary condition at the wavemaker, following the ideas outlined by Shemer & Kit (1988) for the closely related phenomenon of the nonlinear sloshing waves directly excited at the forcing frequency.

In the present work we investigate the long-time evolution of cross-waves in an experimental facility where the dissipation rate at the wavemaker can be varied. This enables us to study, in particular, the similarities and the differences between the two types of resonant nonlinear standing wave in a rectangular tank, i.e. the sloshing waves directly excited at the forcing frequency (Kit, Shemer & Miloh 1987; Shemer & Kit 1988), as compared to the much more complicated parametrically generated subharmonic cross-waves. The experiments are performed at three cross-wave modes, and for a wide range of forcing amplitudes and frequencies. Numerical solutions corresponding to these experimental parameters, are obtained. Special attention is paid to the question of the conditions necessary to sustain the nonlinear cross-waves. This question has not been addressed before in experimental or in theoretical works dealing with cross-waves. The comparison between the numerical and the experimental results leads to certain conclusions regarding the limitations of the theoretical model. It is shown that breaking of steep cross-waves has to be accounted for in the model in order to obtain agreement with the experiment.

2. Model equations

The model equations describing the time and the space evolution of cross-waves in an inviscid fluid and the corresponding boundary condition at the wavemaker, were first obtained by Jones (1984). The equations of Jones were shown to be equivalent to a familiar nonlinear Schrödinger (NLS) equation (Miles 1985). Miles has indicated that a sign error existed in the original definition of the detuning coefficient λ in the derivation of Jones. Miles & Becker (1988) have rederived the governing equation, using the Lagrangian formulation of the problem. Lichter & Chen (1987) have also rederived the NLS equation for the resonant cross-waves, and reported on some differences with Jones in the definition of equation coefficients. Taking into account this controversy and in order to perform quantitative comparison between the experimental and the theoretical results, we have derived the NLS equation and the wavemaker boundary condition again, following the lines of Kit *et al.* (1987). Our result in the absence of dissipation was identical to the expressions obtained by Jones, if the correction of Miles (1985) is taken into account. Following Shemer & Kit (1988), we also take into account in our model dissipation along the tank and at the wavemaker.

We consider a deep rectangular tank with the side walls at $y = 0$ and $y = b$, equipped with the wavemaker at one end, $x = 0$, and with the mean water level at $z = 0$, z being directed upward. The channel width b and the characteristic time scale $(b/g)^{\frac{1}{2}}$, g being the acceleration due to gravity, were used to render all variables dimensionless. The wavemaker operates at the forcing frequency Ω, the subharmonic of which, $\omega = \frac{1}{2}\Omega$, is the frequency of the nth mode cross-waves and is close to the deep-water resonant value $\omega_n = (n\pi g/b)^{\frac{1}{2}}$. The wavemaker surface location, $x = \xi(z, t)$, is given by

$$x = \xi(z, t) = \tfrac{1}{2}sF(z)\,(\mathrm{i}\,\mathrm{e}^{-\mathrm{i}\Omega t} + *), \tag{1}$$

s being the wavemaker amplitude at mean free surface level and $F(z)$ the wavemaker amplitude shape function, defined so that $F(0) = 1$. The small parameter of the problem, ϵ, is proportional to s, and is defined by

$$\epsilon = \frac{1}{(n\pi)^{\frac{1}{2}}} \frac{s}{b} f_n, \tag{2}$$

where f_n depends on $F(z)$,

$$f_n = -2F(0) + 4n\pi \int_{-\infty}^{0} F(\zeta)\,\mathrm{d}\zeta + \int_{-\infty}^{0} \mathrm{e}^{2n\pi\zeta} \frac{\mathrm{d}F}{\mathrm{d}\zeta}\,\mathrm{d}\zeta. \tag{3}$$

For the shape function of the hinged wavemaker installed in our experimental facility, we obtain from (2) and (3) the following working expressions for the cross-wave modes investigated in the present work: for the second mode, $f_2 = 4.44$, $\epsilon_2 = 1.77\, s/b$; for the third mode, $f_3 = 7.53$, $\epsilon_3 = 2.45\, s/b$ and for the fifth mode, $f_5 = 13.77$, $\epsilon_5 = 3.47\, s/b$.

With the value of ϵ known, one obtains the relations between the normalized slow variables of the problem and the corresponding physical values. The slow time T and length X variables are defined as:

$$T = \epsilon^2 \tfrac{1}{4} (n\pi)^{\frac{7}{2}} \frac{t}{(b/g)^{\frac{1}{2}}}, \quad X = \epsilon (n\pi)^{\frac{5}{2}} \frac{x}{b}. \tag{4a,b}$$

The detuning parameter λ has the following form:

$$\lambda = \frac{2}{(n\pi)^4} \left[\frac{\omega^2 - \omega_n^2}{\epsilon^2} \frac{b}{g} + \frac{19 - 5\sqrt{17}}{4 f_n^2} \right]. \tag{5}$$

The frequency-independent portion of λ, which is due to the cross-waves interacting with the progressive wave field along the tank, is usually negligible and decreases with increasing mode number n. The maximum value of this correction for the lowest mode employed in the present experiments, $n = 2$, is 0.02. The normalized dimensionless potential amplitude $C(X, T)$ is related to the dimensional cross-wave potential ϕ by

$$\phi = \epsilon (b^3 g)^{\frac{1}{2}} \exp\left(\frac{n\pi z}{b}\right) \cos\left(\frac{n\pi y}{b}\right) [C(X, T)\, \mathrm{e}^{-\mathrm{i}\omega t} + *]. \tag{6}$$

The governing NLS equation for the complex cross-wave velocity potential amplitude C has the following form:

$$\mathrm{i} \frac{\partial C}{\partial T} + \frac{\partial^2 C}{\partial X^2} + (\lambda + a_1) C + 2|C|^2 C = 0, \tag{7}$$

with the homogeneous boundary condition at the wavemaker

$$\frac{\partial C}{\partial X} = \mathrm{i} C^* - a_2 C, \tag{8}$$

where a_1 and a_2 are the complex dissipation coefficients along the tank and at the wavemaker, respectively. Note that both the absolute values and the arguments of these complex coefficients can be calculated for purely molecular dissipation, Shemer & Kit (1988). The values obtained from the appropriate equations are, however, substantially lower that those estimated by Lichter & Chen (1987) and Kit & Shemer

(1989) from the neutral stability experiments by Barnard & Pritchard (1972) and by Shemer & Lichter (1987). The physical reasons for this discrepancy are discussed in detail by Kit & Shemer.

3. Experimental and numerical procedures

Experiments were carried out in a rectangular wave tank which is 18 m long, 1.2 m wide and filled to a mean water depth of 0.6 m. The tank is equipped by a modular wavemaker. The detailed description of the experimental facility and the data acquisition procedure were presented in Shemer, Kit & Miloh (1987) and Kit *et al.* (1987). The wavemaker was driven by a computer-generated signal. The sampling interval in each record was selected so that 32 data points were sampled during the forcing period, thus giving 64 data points per cross-wave period. The amplitude and the phase of the cross-wave were calculated from these records for each subharmonic period. The experimentally obtained dependence of cross-wave amplitudes on time was usually slightly smoothed in graphic presentation using the running average procedure. The total duration of each record was chosen in accordance with the long-time behaviour of the wave field.

The variation of dissipation rate at the wavemaker in the present work was done by applying roughness elements (steel angles) at the wavemaker surface. Details of wavemaker geometry with and without these roughness elements were discussed in detail by Shemer & Kit (1988).

Equation (7) with the boundary condition at the wavemaker (8) was solved numerically by the semi-implicit Crank–Nicholson scheme, with the evaluation of the nonlinear term performed using the suggestion by Aranha, Yue & Mei (1982). The domain of calculations was large enough to eliminate the influence of the far end. The homogeneous boundary condition at the wavemaker was treated by separation of the real and the imaginary parts, which was necessary because of the presence of the complex conjugate term in (8). In most cases, the computations were performed with the timestep $\Delta T = 0.02$ and the space step $\Delta X = 0.2$. When strong spatial gradients were present in the wave field, smaller integration steps were used. A similar numerical scheme was extensively verified in earlier computations of the long-time evolution of directly generated standing waves in the tank (Kit *et al.* 1987).

When computations were performed with a zero initial condition, a small decaying in time inhomogeneous forcing term in the form of $i\epsilon \exp(-T)$ was added to the right-hand side of (8) in order to provide the initial disturbance. The chosen value of ϵ was usually 0.1. While this initial excitation is different from that used by Lichter & Chen, it does not affect the results after the initial period. In certain runs, a non-zero initial condition was employed. In these cases, the artificial inhomogeneous driving term became unnecessary and the calculations started with the wave field which existed in the tank at the end of the previous run (hot initial condition). This technique made it possible to study numerically the hysteresis observed in the experiments.

4. Verification of scaling

The scaling of the dimensionless variables in the present work is identical to that suggested by Jones (1984). Lichter & Chen questioned the suitability of this scaling for the long-time evolution analysis of nonlinear cross-waves. A convenient way to check the validity of the adopted scaling procedure is to calculate the ratio of the

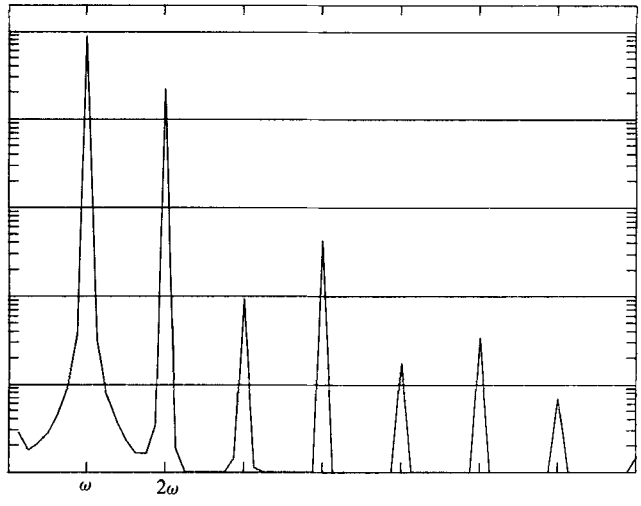

FIGURE 1. The power spectrum of the surface elevation at $X = 0.3$; $n = 3$, $\lambda = 0$.

amplitudes of the progressive wave at the frequency of forcing, $a_{\rm pr}$, and the standing cross-wave of the nth mode at the subharmonic frequency, a_n, and compare it with the appropriately scaled experimentally measured values. The amplitude of the cross-wave, a_n, is obtained from the velocity potential, see (6), while $a_{\rm pr}$ for deep water is given by the linear theory (Havelock 1929). The resulting expression for the geometry of our facility has the following form:

$$\frac{a_{\rm pr}}{a_n} = \frac{1}{f_n|C(X,T)|}. \tag{9}$$

Comparison of the directly measured ratio between the amplitudes of the progressive and the cross-waves with the normalized according to (6) cross-wave amplitude, which depends on the chosen expression for the small parameter (2), could thus serve as a tool for verification of the scaling procedure.

Figure 1 shows the experimentally measured power spectrum of the surface elevation close to the wavemaker for the cross-waves of the third mode. The energy density ratio between the subharmonic and the forcing frequencies in this figure equals 4.0, in a very good agreement with the amplitude ratio between the standing subharmonic cross-wave and the propagating wave at the frequency of forcing, calculated from (9), which for $n = 3$ and $|C| \approx 0.3$, gives the value of ≈ 2.25. This observation supports the validity of the scaling procedure suggested by Jones (1984) and adopted in the present work.

5. Long-time evolution of cross-waves

When the resonant standing waves in a rectangular tank are excited directly by a wavemaker having a typical lengthscale equal to the wave-length of the standing wave, it is possible to obtain very good qualitative and quantitative agreement between the experimental results and the numerical solutions of the NLS equation (7) for a wide range of forcing conditions, when the dissipation coefficients along the tank and at the wavemaker are properly chosen (Shemer & Kit 1988). The question whether the substantially more complicated physical mechanism of parametric

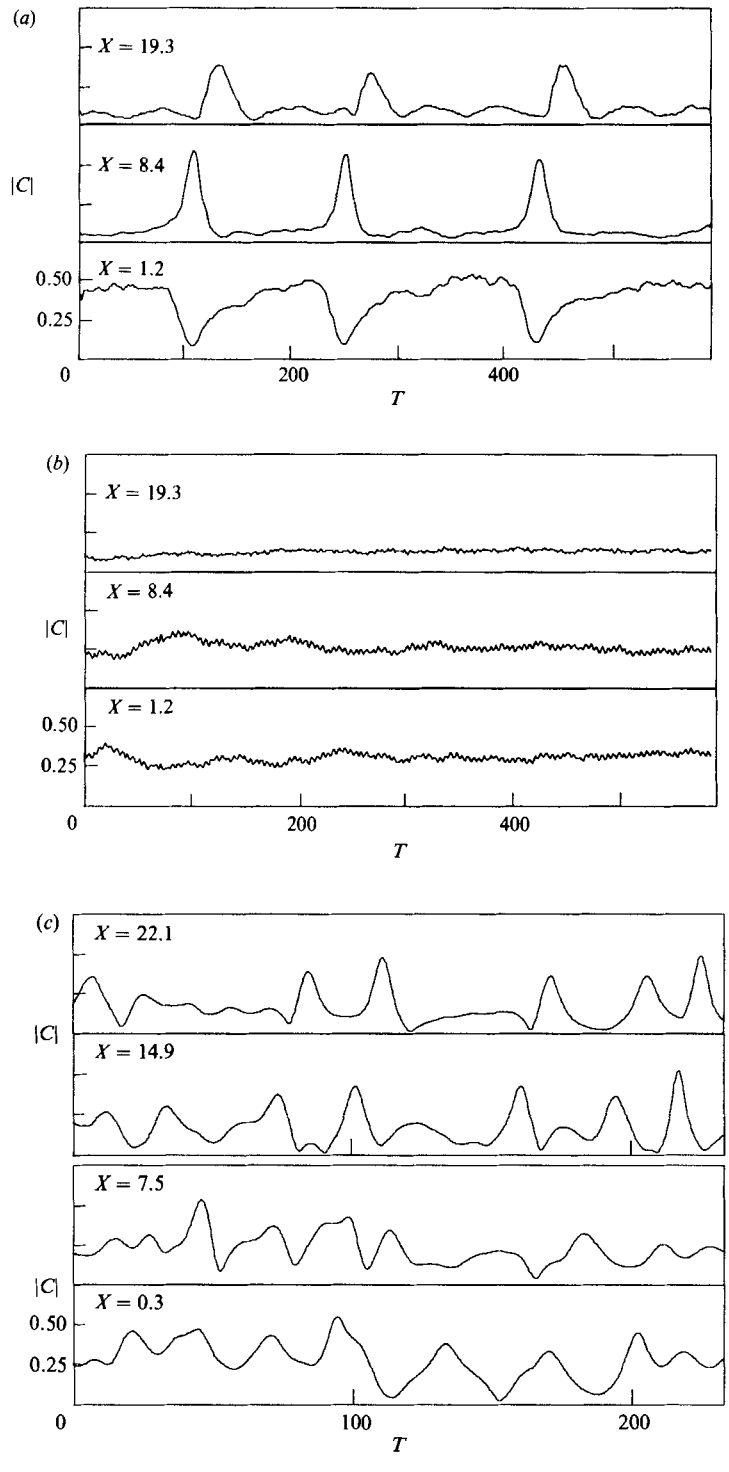

FIGURE 2. Long-time modulation patterns observed in the experiments: (*a*) $n = 5$; $\epsilon = 1.36 \times 10^{-2}$, $\lambda = -0.10$; higher dissipation rate at the wavemaker, (*b*) as in (*a*), but lower dissipation rate at the wavemaker; (*c*) $n = 3$, $\epsilon = 1.21 \times 10^{-2}$, $\lambda = -0.1$.

excitation can be grasped satisfactorily by the model NLS equation (7) with the homogeneous boundary condition at the wavemaker (8), remained open and is thus of special interest. In order to provide an answer to this question, extensive measurements of cross-waves at various forcing conditions and three different modes were performed. This experimental study was accompanied by numerical solutions of the model equations with appropriate dissipation coefficients.

5.1. *Experimental results*

The possibility of obtaining a rich variety of evolution patterns of cross-waves was demonstrated by Shemer & Lichter (1987) who performed experiments in the present facility for $n = 5$ and high dissipation rate at the wavemaker (with the roughness elements attached to its surface). In this work we limit ourselves to presenting only a few selected long-time evolution figures out of a substantial body of accumulated experimental data, which contribute to a deeper understanding of physical processes in nonlinear cross-waves.

The results obtained for the cross-waves of the fifth mode at both dissipation rates at the wavemaker and at identical values of $\lambda = -0.10$ and of $\epsilon = 0.0136$, are given in figure 2(a, b). The pattern obtained at the higher dissipation rate is characterized by the quasi-periodic appearance of solitons, while at the lower dissipation rate no such solitons appeared. Note that at the fifth cross-wave mode, no solitons could be observed at the lower dissipation rate at the wavemaker in the whole range of existence of cross-waves. These results show the essential influence of dissipation at the wavemaker on the cross-wave regime in the tank. In this sense cross-waves therefore appear to be similar to the directly excited sloshing waves (Shemer & Kit 1988).

In the experiments at the third mode with a smooth wavemaker, strong non-periodic modulations in time, occasionally resembling soliton appearance, were obtained at $\lambda = 0$, $\epsilon = 0.0121$ (figure 2c). The focusing of the wave energy seems to increase with the distance from the wavemaker. The details of slow-time modulation of cross-waves, presented in figure 2, thus show much more complicated patterns in comparison with the nearly perfectly periodic modulation of the directly excited sloshing waves. At lower values of $\lambda (\lambda < -0.45)$, nearly steady trapped cross-waves were observed, as was the case for the fifth mode.

A convenient way to summarize the bulk of information regarding the time dependence of cross-wave amplitudes, is to present, as a global characteristic of the wave field, the variation of the long-time averaged amplitude of the cross-waves with the detuning parameter λ (figure 3a), and, as a characteristic of the depth of modulation at a slow timescale, the r.m.s. value of the modulated amplitude, normalized by its mean value (figure 3b).

At high dissipation rate at the wavemaker and $n = 5$, a well-defined frequency exists, at which transition between the steady and the modulated cross-wave regimes occurs (Shemer & Lichter 1987). Our analysis of their raw experimental data shows that for three forcing amplitudes employed, $\epsilon = 0.0136$, $\epsilon = 0.0144$ and $\epsilon = 0.0176$, the transitional value of λ was close to -0.11 in all cases. In the present experiments at lower wavemaker dissipation rate (without roughness elements), no such distinct transition was observed. Transition from the quasi-steady cross-wave regime at low values of λ to a strongly modulated wavefield at higher forcing frequencies, can be seen clearly in figure 3(b) only for the third mode. In the quasi-steady regime ($\lambda < -0.45$), the amplitude fluctuations relative to the mean r.m.s. value did not exceed a few per cent, while in the modulated regime this quantity attained values

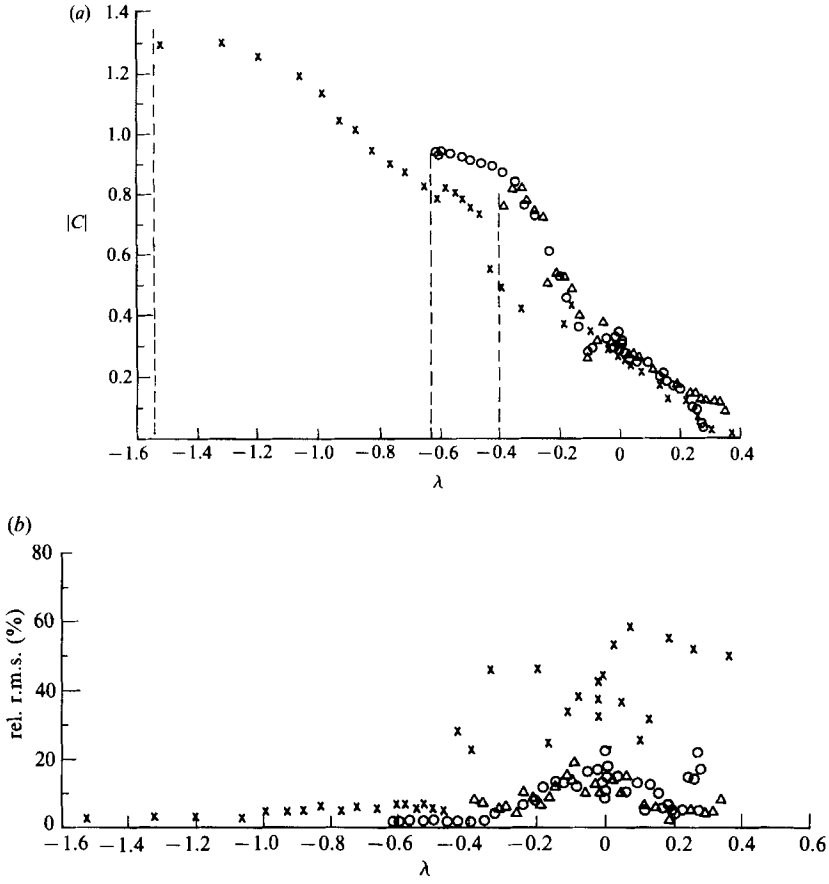

FIGURE 3. The variation with λ of (*a*) the long-time averaged cross-wave amplitude, and (*b*) the r.m.s. of the cross-wave amplitudes, normalized by their mean values; ×, $n = 3$, $\epsilon = 1.21 \times 10^{-2}$; ○, $n = 5$, $\epsilon = 0.943 \times 10^{-2}$; △, $n = 5$, $\epsilon = 1.15 \times 10^{-2}$.

which were higher by an order of magnitude. Note that the data presented in figure 3 is based on averaging the cross-wave amplitudes over the whole duration of sampling. This duration at all cross-wave modes usually corresponded to 240 periods of cross-waves, being longer in some experimental runs. For example, the modulation pattern presented in figure 2 represents 720 periods of cross-waves. One can see from this figure that the characteristic times of slow modulation may become comparable with the total duration of sampling. The scatter of the data for $\lambda > -0.45$ can be in part attributed to this fact. For cross-waves of the fifth mode, the depth of modulation is notably lower than in the case of the third mode, and the transition between the region of relatively strong modulation and that of an essentially steady regime, is not as sharp as in the previous case, and occurs at $-0.35 < \lambda < -0.1$, for both amplitudes of forcing.

5.2. *Selection of the dissipation coefficients in the theoretical model*

The results of two earlier investigations in the present experimental facility served as guides for the choice of the dissipation coefficients in the numerical study. The first is the research on the role of dissipation in the time evolution of directly excited sloshing waves (Shemer & Kit 1988), while the other is the analysis of the relation

between the dissipation and the neutral stability of cross-waves (Kit & Shemer 1989). Both these studies correspond to conditions which are somewhat different from those in the present experiments. The results of the neutral stability study which deals directly with cross-waves, are limited to vanishingly small amplitudes, while the dissipation coefficients estimated from the experiments on the sloshing waves of comparable amplitudes are only distantly related to the present investigation of subharmonic cross-waves. The preliminary estimates of the dissipation coefficients based on these considerations were therefore further redefined by comparing the numerical solutions with experiment.

The dissipation along the tank in our experimental facility is relatively small compared to that at the wavemaker. The absolute value of the dissipation coefficient along the tank, $a_1 = 0.14$ and its argument, $\phi_1 = 45°$ were selected as a reasonable approximation. The dissipation coefficient at the wavemaker, a_2, was chosen to be imaginary, in agreement with Kit & Shemer (1989), and its absolute value adopted here for the fifth mode experiments was $a_2 = 0.5$ at high dissipation rate at the wavemaker and $a_2 = 0.2$ at low dissipation rate. The dissipation coefficient selected for a smooth wavemaker at the third mode was $a_2 = 0.35$. The difference between the dissipation coefficients for the fifth and for the third cross-wave modes stems from the dependence of a_2 on the mode number n (Kit & Shemer 1989):

$$a_2 = \frac{\delta\sqrt{2}}{b\epsilon(\pi n)^{\frac{1}{2}}}, \tag{10}$$

where δ corresponds to the thickness of the boundary layer at a solid wall in the oscillating flow: in the case of purely molecular dissipation δ represents the thickness of the Stokes layer.

5.3. *Numerical computations*

In contrast to the directly excited sloshing waves, cross-waves can be generated essentially from rest by parametric resonance only in a narrow band of the values of the detuning parameter λ. For the selected values of the dissipation coefficients, the cross-waves could be excited from rest in the numerical simulations (using the small artificial homogeneous forcing term as explained in §3) in the following bands: $0.93 < \lambda < 0.63$ for $a_2 = 0.2$; $-0.83 < \lambda < 0.42$ for $a_2 = 0.35$ and $-0.67 < \lambda < 0.22$ for $a_2 = 0.5$. These bands are in accordance with the results which can be calculated based on the neutral stability study of Kit & Shemer (1989). In experiments, cross-waves were indeed excited within these bands.

For all sets of dissipation coefficients stationary wave patterns were obtained in the numerical calculations at sufficiently low values of λ, while at higher λ the wavefield was modulated. Various types of modulation obtained in computations are presented in figure 4. In figures 4(*a*) and 4(*b*) the wavefield is shown at identical values of the detuning parameter $\lambda = -0.2$ and for different dissipation coefficients at the wavemaker. While at higher dissipation at the wavemaker (figure 4*a*) soliton-type modulations somewhat resembling the patterns observed in the experiments were obtained, the modulation at lower values of a_2 (figure 4*b*) is quite different from that of figure 4(*a*). It should be stressed that for $n = 5$ and low dissipation rate at the wavemaker, no solitons were obtained at any values of λ in the numerical computations or in the experiments. At slightly higher values of a_2 (figure 4*c*), wave patterns vaguely resembling chaotic appearance of solitons in the experiments at the third mode were obtained at $\lambda = -0.4$ (cf. figure 2*c*).

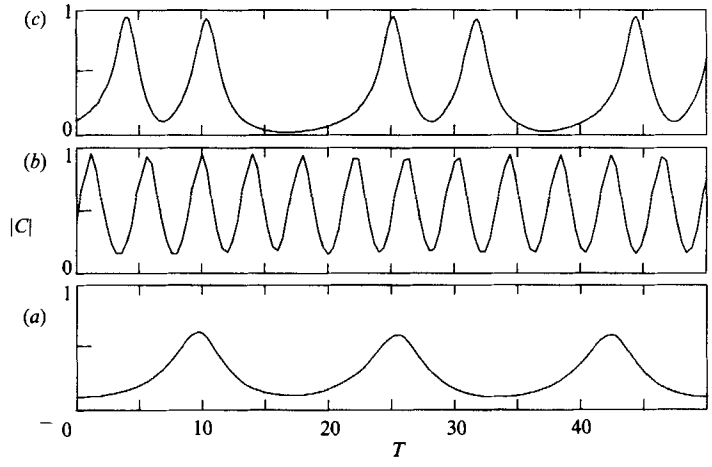

FIGURE 4. Long-time modulation of cross-waves obtained in numerical experiments, $X = 1$; $a_1 = 0.14$, $\phi_1 = 45°$; (*a*) $a_2 = 0.5$, $\lambda = -0.2$; (*b*) $a_2 = 0.2$, $\lambda = -0.2$; (*c*) $a_2 = 0.35$, $\lambda = -0.4$.

It is thus clear from the results of this section that the agreement between the experimental and the numerical results in the case of the parametrically excited cross-waves is quite poor when compared to the directly generated sloshing waves. This reflects, as was stressed by Jones (1984), the substantially more complex physical nature of the cross-waves which are excited by self-interactions defined by the implicit homogeneous boundary condition (8), in contrast to relatively straightforward direct generation of sloshing waves, caused by an explicit inhomogeneous driving term in the wavemaker boundary condition.

6. Regions of cross-wave existence

As follows from the results presented in the previous section, cross-waves were observed in the experiments in a limited range of variation of the detuning parameter λ. It should be stressed here that in the experiments, the cross-waves were excited at the initial stage at the most unstable frequency. The forcing frequency was then gradually varied, while keeping the wavemaker amplitude constant, and the measurements at each frequency were performed until no cross-waves could be observed in the tank. By this technique, cross-waves could be experimentally obtained at the values of the detuning parameter λ at which no parametric excitation was possible without there being a strong enough cross-wave field already present in the tank. For example, at the second cross-wave mode, no cross-waves appeared in the tank when the wavemaker was operated from rest at values of λ beyond the range $-0.5 < \lambda < 0$, while with hot initial condition, cross-waves existed even for $\lambda < -3$, and only at $\lambda = -3.6$ did cross-wave field breakdown occur.

A similar technique was therefore employed in the numerical experiments. In the presence of a small initial disturbance, cross-waves could be excited only at the values of λ within the range of the linear instability, as defined by the neutral stability curves obtained for appropriate dissipation conditions by Kit & Shemer (1989). Computations of the cross-wave field with the initial hot conditions, i.e. starting with the wave field obtained numerically at a close value of λ, indeed showed the possibility of sustaining cross-waves at the detuning coefficients λ lower than the smallest value predicted by the linear theory.

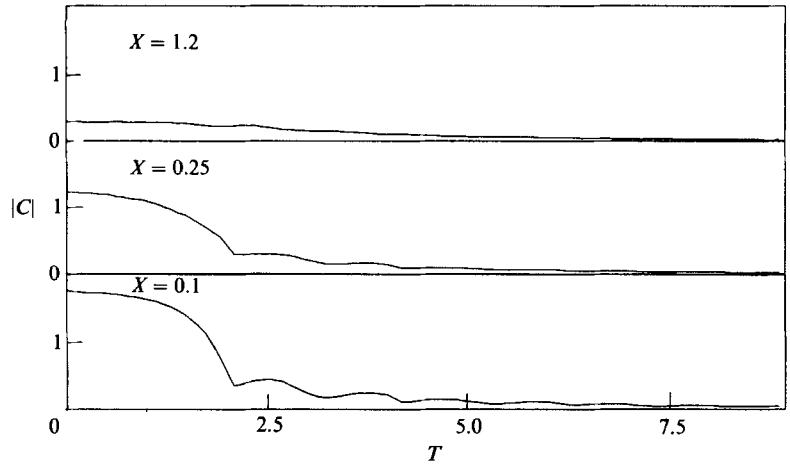

FIGURE 5. The breakdown of the second mode cross-wave field, $\epsilon = 1.36 \times 10^{-2}$, $\lambda = -3.6$.

6.1. *Physical reasons for the breakdown of the cross-wave field*

In the experiments, the gradual reduction of the frequency of forcing was accompanied by an increase of the wave amplitude at the wavemaker, while the extent of the region with noticeable cross-wave amplitude decreased, so that the whole wave field became restricted to the vicinity of the wavemaker. Further decrease in the forcing frequency resulted in a dramatic breakdown of the cross-wave field. Such a breakdown was recorded in the experiments at the second mode and is shown in figure 5. It is important to note that at all forcing amplitudes and for all three cross-wave modes investigated in the present work, breaking of cross-waves in the vicinity of the wavemaker was always observed at forcing frequencies preceding the breakdown value. A photograph of the violent breaking of these extremely steep waves was presented in figure 6 of Lichter & Shemer (1986).

The whole range of existence of nonlinear cross-waves is clearly seen in figure 3(*a*). In all cases cross-wave amplitudes gradually decrease with increasing λ, and the waves practically vanish at $\lambda \approx 0.3$. At the low end, on the other hand, a substantial difference exists between various modes and amplitudes of forcing. At the third mode, cross-waves break down at $\lambda_{cr} \approx -1.6$, which is significantly higher than the corresponding value for the second mode ($\lambda_{cr} = -3.6$, see figure 3). For the higher fifth mode, cross-waves disappear at $\lambda_{cr} = -0.62$ for $\epsilon = 0.943 \times 10^{-2}$ and $\lambda_{cr} = -0.40$ for $\epsilon = 1.15 \times 10^{-2}$. The corresponding maximum values of $|C|$ just before the breakdown are also different.

In the numerical simulations, when the detuning parameter was gradually decreased, the cross-wave amplitude at the wavemaker increased indefinitely. This phenomenon was accompanied by the shrinking of the wave field to the close vicinity of the wavemaker and by fast decay of the wave amplitude with the distance from the wavemaker. While this is in qualitative agreement with the experiment, no breakdown of cross-waves could be obtained numerically without introducing modifications to the model.

6.2. *Steepness of the cross-waves and scaled variables*

In the adopted theoretical model, the detuning parameter λ is the only dimensionless variable parameter. The results of figure 3(*a*) indeed show a pronounced trend of

n	ϵ	$\Delta k/k_n$	λ_{cr}	$k_n a$	$\lvert C\rvert_{max}$
5	0.0943×10^{-2}	−0.106	−0.62	1.01	0.94
5	1.15×10^{-2}	−0.104	−0.40	1.08	0.76
3	1.21×10^{-2}	−0.094	−1.53	0.90	1.29
2	1.36×10^{-2}	−0.083	−3.60	0.83	1.94

TABLE 1. The experimentally measured parameters on the verge of cross-wave field breakdown

collapse of the measured dependence of $|C|$ on λ for different experimental conditions. The similarity in the dependence $|C| = |C(\lambda)|$, however, is restricted to relatively high values of the detuning coefficient. Both the breakdown values λ_{cr} and the maximum possible amplitudes $|C|_{max}$ obtained in the experiments appear to be quite different for various ϵ and n. One should keep in mind that wave breaking dominates the wave field in the vicinity of the wavemaker at these high values of $|C|$. We present here the corresponding experimentally measured values of the maximum standing wave steepness, $k_n a$, where k_n is the wavenumber of the resonant cross-wave of the nth mode. The extreme conditions at which cross-waves were observed in the present experiments, are summarized in table 1. The maximum recorded values of $k_n a$ significantly exceeded the maximum theoretical value for finite stationary waves of permanent form in a perfect fluid, which is equal to 0.685 (Penney & Price 1952). For example, for the fifth cross-wave mode, $k_5 a = 1.10$ was obtained for the forcing amplitude $\epsilon = 0.943\times10^{-2}$, and $k_5 a = 1.18$ for $\epsilon = 0.115\times10^{-1}$.

The maximum wave steepness $(k_n a)_{max}$ thus remains approximately constant for all cases studied. It seems physically reasonable to assume that owing to breaking, a universal limiting value of the maximum possible standing wave steepness actually exists. Employing (6) and the linearized boundary condition at the free surface, the following relation between the dimensional wave amplitude a and $|C|$ is obtained: $a/b = 2\epsilon(\pi n)^{\frac{1}{2}}|C|$. From here it follows immediately that

$$2\epsilon(\pi n)^{\frac{3}{2}}|C|_{max} = (k_n a)_{max} \approx \text{const}, \tag{11}$$

which can explain the experimentally observed dependence of $|C|_{max}$ on both ϵ and the mode number n.

The definition of λ (5) can be rewritten in the following way

$$\lambda = \frac{2\Delta k/k_n}{\epsilon^2(\pi n)^3}, \tag{12}$$

where the negligible contribution due to the progressive wave is omitted, and Δk is the deviation of the wavenumber corresponding to the subharmonic of the forcing frequency, from the resonant value k_n. Comparing (11) and (12) yields

$$\frac{\lambda_{cr}}{|C|^2_{max}} = \frac{8\Delta k_{cr}/k_n}{(k_n a)_{max}}. \tag{13}$$

The experimentally observed values of $\Delta k_{cr}/k_n \approx 0.10$ and $(k_n a)_{max} \approx 1.0$ remain approximately constant for all cases investigated, see table 1. The value of $\lambda_{cr}/|C|^2_{max}$, which can also be calculated from the data presented in the table, does not differ notably from 0.8, in accordance with (13).

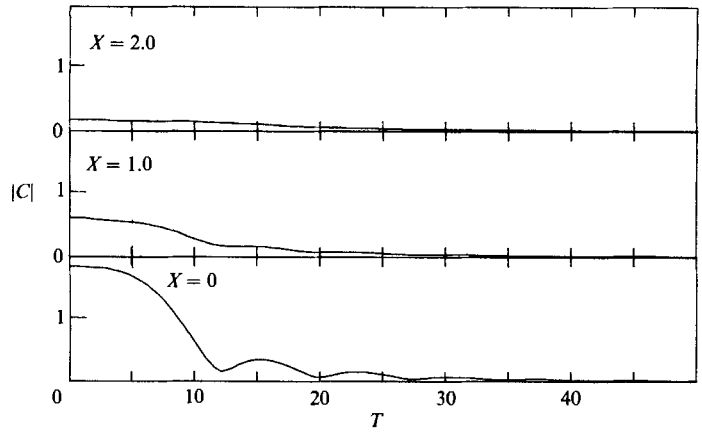

FIGURE 6. The breakdown of the cross-wave field, obtained numerically. $\lambda = -1.8$, initial wave field was obtained at $\lambda = -1.7$, $|C|_{\max} = 1$, dissipation coefficients as in figure 4(*c*).

$\lvert C\rvert_{\max}$	λ_{cr}	$\lambda_{cr}/\lvert C\rvert^2_{\max}$
1.0	−1.18	1.18
1.2	−1.35	0.94
1.7	−3.5	1.21
2.0	−4.9	1.22

TABLE 2. The breakdown parameters obtained in the numerical experiments ($a_1 = 0.14$, $\phi_1 = 45°$, $a_2 = 0.35$)

6.3. *Modification of the theoretical model*

These experimental results naturally suggest a limitation which can be introduced into the theoretical model in order to account for the wave breaking. There exists a maximum possible value of $|C|$, which is related by (13) to the maximum wave steepness $k_n a$ in the presence of breaking. At each subsequent timestep in the numerical integration the obtained values of $|C(X)|$ were compared with the selected limiting value of $|C_{\max}|$, and at those grid points where the absolute value of $C(X)$ exceeded this threshold, it was replaced by $|C_{\max}|$, while the argument was retained. Although this approach is quite crude, it appears to retain the basic integral properties of the wavefield and drastically improves the agreement between the numerical solutions and the experimental observations. Incorporation of the restriction on $|C|$ in the model equations leads to the disappearance of the cross-wave field at certain value of λ, see figure 6, in a similar manner to the experimental observations, as recorded in figure 5, albeit with a different characteristic time. For any given limiting value of $|C|_{\max}$ accepted in the computations, the corresponding breakdown detuning coefficient λ_{cr} was obtained in the computational runs. The results of numerous computational runs summarized in table 2 resemble closely the experimental data. The values of $\lambda_{cr}/|C|^2_{\max}$ obtained numerically are close to unity and exceed slightly the corresponding experimental values.

The reasons for the relation between λ_{cr} and $|C|_{\max}$ can be heuristically seen from the following considerations. In the governing equation (7), the value of $(\lambda + 2|C|^2)$ can be interpreted as a coefficient of the linear term. The analysis of the neutral

stability curves in the presence of the dissipation at the wavemaker shows that the instability region does not extend beyond small positive values of λ (Kit & Shemer 1989). One can thus deduce that λ_{cr} is roughly proportional to $|C|^2_{max}$. While the nonlinear term and wave breaking play the decisive role in the cross-wave behaviour at low values of λ, the high-frequency end of the range of cross-wave existence can be seen as essentially linear, since the wave amplitudes gradually decrease with increasing λ, both in the experiments and in the numerical computations.

7. Concluding remarks

In the present work we report on extensive experimental and numerical investigations of parametrically excited cross-waves in a rectangular tank. The results presented here reveal that not only the dissipation along the tank, but also the dissipation at the wavemaker may be of importance in some experimental facilities. Both dissipation mechanisms were incorporated in the model by using appropriate complex dissipation coefficients in the governing equation and in the wavemaker boundary condition. Special attention was paid to the regions of existence of cross-waves. It was shown that due to nonlinear effects, cross-waves can be sustained at the values of the detuning coefficient far below the neutral stability limits. A sharp breakdown of the cross-wave field at low forcing frequencies was revealed in the present study and was attributed to the breaking of the steep cross-waves. The limit on the cross-wave amplitude due to breaking was introduced into the model and allowed to obtain numerically the values of the detuning parameter λ_{cr} at which this cross-wave field cannot sustain itself anymore. In this sense not only qualitative, but also quantitative agreement with the experiment is quite satisfactory.

Jones (1984) indicated that the NLS equation can only describe correctly the experiment when damping is taken into consideration. Lichter & Chen (1987), indeed, obtained good quantitative agreement between their numerical solution of the NLS equation and the experiment of Barnard & Pritchard (1972). Lichter & Chen perform their comparison of the numerical and experimental results in the presence of very strong dissipation along the tank, estimated from the neutral stability by Barnard & Pritchard and at a single value of the forcing frequency. In reality, however, the dissipation mechanisms depend strongly on the existing wave field, and we doubt that a single dissipation coefficient can describe properly the whole variety of existing wave patterns. Even when complex dissipation coefficients along the tank and at the wavemaker are taken into account and limitations on wave amplitude caused by the wave breaking are accounted for as well, only qualitative agreement between the wave patterns observed in a wide range of experimental conditions and the results of the corresponding numerical computations, could be obtained. In spite of these reservations, the suggested model, which incorporates both nonlinear and damping effects, appears to grasp correctly the major physical mechanisms governing the long-time evolution of cross-waves and provides a useful tool for describing the region of their existence.

This work was supported in part by the US–Israel Binational Science Foundation grant no. 85-00343. We are grateful to the reviewers for their constructive remarks, which helped to improve this paper.

REFERENCES

ARANHA, J. A., YUE, D. K. P. & MEI, C. C. 1982 Nonlinear waves near a cut-off frequency in an acoustic duct – a numerical study. *J. Fluid Mech.* **121**, 465–485.

BARNARD, B. J. S. & PRITCHARD, W. G. 1972 Cross-waves. Part 2. Experiments. *J. Fluid Mech.* **55**, 245–255.

GARRETT, C. J. R. 1970 On cross-waves. *J. Fluid Mech.* **41**, 837–849.

HAVELOCK, T. H. 1929 Forced surface waves on water. *Phil. Mag.* **8**, 569–576.

HOCKING, L. M. 1987 The damping of capillary–gravity waves at a rigid boundary. *J. Fluid Mech.* **179**, 253–266.

JONES, A. F. 1984 The generation of cross-waves in a long deep channel by parametric resonance. *J. Fluid Mech.* **138**, 53–74.

KIT, E. & SHEMER, L. 1989 On the neutral stability of cross-waves. *Phys. Fluids* **A 1**, 1128–1132.

KIT, E., SHEMER, L. & MILOH, T. 1987 Experimental and theoretical investigation of nonlinear sloshing waves in a rectangular channel. *J. Fluid Mech.* **181**, 265–291.

LICHTER, S. & CHEN, J. 1987 Subharmonic resonance of nonlinear cross-waves. *J. Fluid Mech.* **183**, 451–465.

LICHTER, S. & SHEMER, L. 1986 Experiments on nonlinear cross waves. *Phys. Fluids* **29**, 3971–3975.

MAHONY, J. J. 1972 Cross-waves. Part I. Theory. *J. Fluid Mech.* **55**, 229–244.

MEI, C. C. & LIU, L. F. 1973 The damping of surface gravity waves in a bounded liquid. *J. Fluid Mech.* **59**, 239–256.

MILES, J. W. 1984 Parametrically excited solitary waves. *J. Fluid Mech.* **148**, 451–460.

MILES, J. W. 1985 Note on a parametrically excited, trapped cross-wave. *J. Fluid Mech.* **151**, 391–394.

MILES, J. W. & BECKER, J. 1988 Parametrically excited, progressive cross-waves. *J. Fluid Mech.* **186**, 129–146.

PENNEY, W. G. & PRICE, H. T. 1952 Part II. Finite periodic stationary gravity waves in a perfect fluid. *Phil. Trans. R. Soc. Lond* A **244**, 254–284.

SHEMER, L. & LICHTER, S. 1987 Identification of cross-wave regimes in the vicinity of a cut-off frequency. *Phys. Fluids* **30**, 3427–3433.

SHEMER, L. & KIT, E. 1988 Study of the role of dissipation in evolution of nonlinear sloshing waves in a rectangular channel. *Fluid Dyn. Res.* **4**, 89–105.

SHEMER, L., KIT, E. & MILOH, T. 1987 Measurements of two- and three-dimensional waves in a channel, including the vicinity of cut-off frequencies. *Exps Fluids* **5**, 66–72.